Dark current analysis of mesa type $In_{0.83}Ga_{0.17}As$ p−i−n photodiodes with different annealing treatment

Li Ping[1,2,3], Li Tao[1,2], Deng Shuangyan[1,2], Li Xue[1,2], Shao Xiumei[1,2], Tang Hengjing[1,2], Gong Haimei[1,2]

(1. State Key Laboratories of Transducer Technology, Shanghai Institute of Technical Physics, Chinese Academy of Sciences, Shanghai 200083, China; 2. Key Laboratory of Infrared Imaging Materials and Detectors, Shanghai Institute of Technical Physics, Chinese Academy of Sciences, Shanghai 200083, China; 3. University of Chinese Academy of Sciences, Beijing 100049, China)

Abstract: In order to study the dark current of the devices, in this paper, the dark current of $In_{0.83}Ga_{0.17}As$ p−i−n photodiodes was analyzed. Extended wavelength $In_{0.83}Ga_{0.17}As$ p−i−n photodiodes with mesa type configuration were fabricated by two different processes. The first process (device marked M135L−5) was: rapid thermal annealing (RTA) was performed after mesa etching. The second process (device marked M135L−3) was: RTA was performed before mesa etching. Dark current mechanisms for extended wavelength $In_{0.83}Ga_{0.17}As$ p−i−n photodiodes with different device fabrication processes were studied by means of the current−voltage curves at different temperatures and bias voltages. In contrast to M135L−5, M135L−3 had a lower dark current at the same test temperature from 220 K to 300 K. The ratio of perimeter-to-area(P/A) was used to characterize the perimeter-dependent leakage current and the area-dependent leakage current. The results show that M135L−3 has a lower area-dependent leakage current. Activation energy of devices served as a method to estimate the dark current composition was extracted from current-voltage curves. The results indicate that the dark current of M135L−5 is dominated by diffusion current at reverse 0.01−0.5 V bias voltage and at 220−270 K. The dark current of M135L−3 is dominated by diffusion current at 250−300 K as well as dominated by generation recombination current and surface recombination current at reverse 0.01−0.5 V bias voltage and at 220−240 K. Meanwhile, the results of dark current fitting also show the same conclusions. The studies have shown that M135L−3 with annealing treatment and optimization process is better than M135L−5 for reducing dark current because the RTA decrease the bulk dark current.

Key words: rapid thermal annealing; extended wavelength; InGaAs; dark current

CLC number: TN215 **Document code:** A **DOI:** 10.3788/IRLA201645.0520002

不同退火处理的台面型 $In_{0.83}Ga_{0.17}As$ pin 光电二极管暗电流分析

李 平[1,2,3],李 淘[1,2],邓双燕[1,2],李 雪[1,2],邵秀梅[1,2],唐恒敬[1,2],龚海梅[1,2]

(1. 中国科学院上海技术物理研究所 传感技术国家重点实验室,上海 200083;
2. 中国科学院上海技术物理研究所 红外成像材料与器件重点实验室,上海 200083;
3. 中国科学院大学,北京 100049)

收稿日期:2015−10−12; **修订日期**:2015−12−02

基金项目:国家 973 项目(2012CB619200);国家自然科学基金(61205105,61007067,61475179)

作者简介:李平(1987−),男,博士生,主要从事短波红外探测器方面的研究。Email:lp806376231@163.com

导师简介:龚海梅(1965−),男,博士生导师,主要从事航天红外探测器、紫外焦平面等新型探测组件及其抗辐射机理与可靠性技术方面的研究。Email:hmgong@mail.sitp.ac.cn

摘 要：为了研究延伸波长 $In_{0.83}Ga_{0.17}As$ pin 光电二极管的暗电流机制。采用两种不同工艺制备了台面型延伸波长 $In_{0.83}Ga_{0.17}As$ pin 光电二极管。第一种工艺(M135L-5)是：台面刻蚀后进行快速热退火(RTA)。第二种工艺(M135L-3)是：台面刻蚀前进行快速热退火(RTA)。采用 IV 测试，周长面积比(P/A)，激活能和暗电流成分拟合方法对器件暗电流机制进行分析。结果显示，在 220~300 K 之间，M135L-3 器件暗电流低于 M135L-5 器件的，并且具有较低表面漏电流。在-0.01~-0.5 V 之间和 220~270 K 之间，M135L-5 器件的暗电流主要是扩散电流。在 250~300 K 之间，M135L-3 器件的暗电流主要是扩散电流，而在-0.01~-0.5 V 之间和 220~240 K 之间，其暗电流主要是产生复合电流和表面复合电流。与此同时，暗电流成分拟合结果也得出一致的结论。研究表明，在降低器件暗电流方面，M135L-3 器件优于 M135L-5 器件，这主要是因为快速热退火降低了器件的体电流。

关键词：快速热退火； 延伸波长； InGaAs； 暗电流

0 Introductions

Indium(In)-rich $In_xGa_{1-x}As$ ternary material grown on InP substrate by gas source molecular beam epitaxy (GSMBE) is suitable for detector applications in the shortwave infrared band such as hyper-spectral imaging, deep space exploration, and infrared astronomical detection and so on[1-2]. The increase of indium composition can extend the wavelength response to 2.6 μm (x=0.83), while leading to many material defects and poorer device performances due to the lattice mismatch about +2.06% between $In_{0.83}Ga_{0.17}As$ active layer and the InP substrate. Dark current is a key parameter for photoelectric detectors. It should be decreased as far as possible to improve signal to noise ratio (SNR) based on the low background application. For the purposes of improving the photoelectric performance of the In-rich InGaAs shortwave infrared(SWIR) detector, some new structures such as "nBn" structure and P-i-I-N structure proposed by other researchers are useful methods in terms of decreasing the dark current of detectors[3-4]. However, the process technology also plays an important role in fabricating the detectors, decreasing the dark current and improving the properties of photodiodes. For example, the annealing treatment is benefit for decreasing the defects of material, the passivation treatment has an effect on reducing the dark current because it restrained the defects of top surface and sidewall, and the etching process is key process technology for fabrication photodiodes because it is very important[5-6]. In this paper, we will study on the dark current of mesa type $In_{0.83}Ga_{0.17}As$ p-i-n photodiodes with different annealing treatment. The order of annealing treatment has an important influence on improving the performance of photodiodes. Mesa type extended wavelength $In_{0.83}Ga_{0.17}As$ photodiodes have been fabricated and their dark current has been tested by current-voltage (I-V) measurement.

1 Experiments

The p-i-n mesa type InAlAs/$In_{0.83}Ga_{0.17}As$/$In_xAl_{1-x}As$/InP double hetero-structure materials used in our work were grown on a semi-insulating InP(Fe) substrate by Gas Source Molecular Beam Epitaxy (GSMBE). The epitaxy materials consisted of a 0.6 μm (Be-doped) P^+-$In_{0.83}Al_{0.17}As$ cap layer with the doping concentration of about $2\times10^{18}cm^{-3}$, a 1.5 μm i-$In_{0.83}Ga_{0.17}As$ absorption layer(unintentionally doped), and a 2.0 μm Si-doped N^+-$In_xAl_{1-x}As$ linearly grading buffer layer with the doping concentration of 2×10^{18} cm^{-3}. The epitaxy materials are shown in Tab.1. $In_xAl_{1-x}As$ linearly grading layers were used to reduce lattice mismatch and dislocation density of active area.

Tab.1 p-i-n epitaxy materials for photodiodes

Epitaxy layer	Layer thickness/μm	Doping concentration /cm^{-3}
P$^+$-$In_{0.83}Al_{0.17}As$ capping layer	0.6	≥2E18
i-$In_{0.83}Ga_{0.17}As$ absorption layer	1.5	=3E16
N$^+$-InAlAs grading buffer layer	2.0	≥2E18
InP substrate	350	ρ>=1E6Ωcm

The M135L-5 and M135L-3 p-i-n mesa type devices were fabricated based on the above materials. The main processes of M135L-5 are as follow: (1) the mesa was formed by Inductively Coupled Plasma (ICP) etching, (2) fabricated the p-type electrode, (3) rapid thermal annealing (420 ℃ and 40 s, N_2) was performed with rise time of about 10 s and negligible overshoot. (4) the mesa top surface and sidewall were passivated with low-temperature SiN_x deposited by Inductively Coupled Plasma Chemical Vapor Deposition (ICPCVD)(75 ℃), as shown in Fig.1(M135L-5). The M135L-3 was fabricated as follows:(1) fabricated the p-type electrode, (2) rapid thermal annealing (420 ℃ and 40 s, N_2) was performed, (3) the mesa was formed by ICP etching, (4) the mesa top surface and sidewall were passivated with low-temperature SiN_x deposited by ICPCVD(75 ℃), as shown in Fig.1(M135L-3).

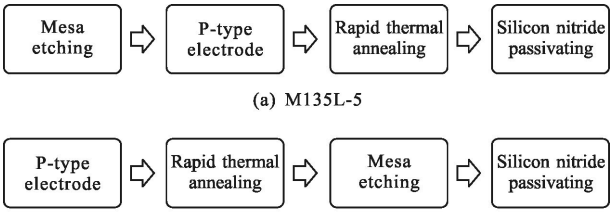

Fig.1 Schemes of fabrication process of mesa type InGaAs photodiode, (M135L-5) rapid thermal annealing after mesa etching, (M135L-3) rapid thermal annealing before mesa etching

Test structures with different photosensitive elements area of Φ200 μm^2, Φ150 μm^2, Φ120 μm^2, Φ100 μm^2, Φ80 μm^2, Φ60 μm^2, Φ50 μm^2, Φ40 μm^2 were designed and fabricated, as shown in Fig.2. Cross-section of the p-i-n mesa type photodiode is shown in Fig.3. The current-voltage curves were measured by Agilent B1500A Semiconductor Device Analyzer at different temperatures, and dark current mechanisms were analyzed according to I-V curves at different temperatures and bias voltages. The ICPCVD SiN_x deposition system is Plasmalab System 100 ICP180 from Oxford Instruments Plasma Technology.

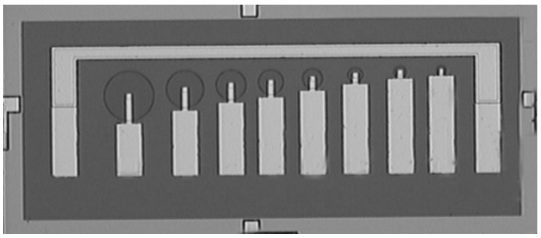

Fig.2 Test structures with different photosensitive elements area

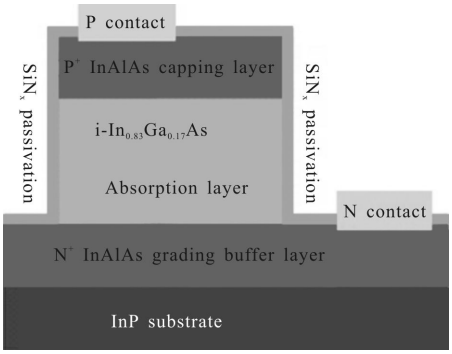

Fig.3 Cross-section of the p-i-n mesa type photodiode

2 Results and discussion

2.1 Theory of dark current mechanism

Dark current is an importance parameter for any photodetectors. In a mesa type p-i-n photodiode, the dark current which has a bad influence on the performance of device originates from several regions: buffer and absorption interface; the absorption layer bulk material; depletion region in absorption; cap and absorption interface; cap and dielectric interface; the dielectric passivation layer; sidewall of the mesa. So the dark current should be decreased immensely to enhance the signal to noise ratio.

At different reverse bias voltage and temperatures, each component plays different roles. The dark current of a pn-junction can be divided into two main sections[7]. The relation between the dark current density

and the ratio of P/A is described by Eq. (1):

$$J=J_s\frac{P}{A}+J_b \tag{1}$$

where J_s is the perimeter-dependent leakage current component, J_b is the area-dependent leakage current component.

The different current mechanisms of extended wavelength InGaAs detectors are considered with the relationship of bias voltage and temperature[8-9]. They are the diffuse current (J_{dif}), the internal generation-recombination (GR) current (J_{gr}), the ohmic leakage current (J_{sh}), the trap-assisted tunneling (TAT) current (J_{tat}), the surface recombination current (J_{sur}), respectively. The relationship of each dark current component is presented as follows:

$$J_{dif}=C_d\exp\left(-\frac{E_g}{kT}\right)\left[\exp\left(\frac{qV}{kT}\right)-1\right]\propto\exp\left(-\frac{E_g}{kT}\right) \tag{2}$$

$$J_{gr}=C_g\exp\left(-\frac{E_g}{kT}\right)(V_{bi}-V)^{1/2}\left[\exp\left(\frac{qV}{kT}\right)-1\right]\propto\exp\left(-\frac{E_g}{kT}\right) \tag{3}$$

$$J_{sh}=\frac{V}{R_{sh}}\propto VT^{3/2}\exp\left(-\frac{E_g}{2kT}\right) \tag{4}$$

$$J_{tat}=\frac{\pi^2q^2WN_tFm_pM^2}{h^3(E_g-E_t)}\exp\left[-\frac{8\pi\sqrt{m_p}\,(E_g-E_t)^{3/2}}{3qhF}\right] \tag{5}$$

$$J_{sur}\propto\sqrt{abs(V)}\exp\left(-\frac{E_g}{4kT}\right) \tag{6}$$

$$J\propto\exp\left(-\frac{E_a}{kT}\right) \tag{7}$$

where C_d and C_g are a constant related to material parameters, E_g is the energy gap of InGaAs absorption layer, k is the Boltzmann constant, V_{bi} is built-in voltage, W is the depletion width, N_t is the trap state density, E_t is the trap energy level, m_p is hole mass, M is a matrix element related to trap potential barrier, F is electric field intensity, E_a is thermal activation energy.

The thermal activation energy E_a of the detector extracted from fitting I-V curves can evaluate the major dark current mechanisms. The thermal activation energy (E_a) is extracted at certain reverse-bias voltage. Dark current mechanisms are dominated by diffusion current when $E_a=E_g$, whereas dominated by internal GR and ohmic leakage current when $E_a=E_g/2$, and dominated by surface recombination current when $E_a=E_g/4$.

2.2 Test results and dark current analysis

The curves of J as a function of P/A for M135L-5 and M135L-3 at room temperature(300 K) are shown in Fig.4. The graph shows that the curve of M135L-3 is lower than M135L-5, indicating the lower area-dependent leakage current component of M135l-3, but the perimeter-dependent leakage current of M135L-3 is higher obviously. The fitted J_s and J_b values at room temperature and -10 mV bias for M135L-3 and M135L-5 are shown in Fig.4, respectively. The results show that J_s value of M135L-5 (6.635E-9 A/cm) is lower than that of M135L-3 (1.157E-7 A/cm), indicating that the perimeter-dependent leakage current of M135L-5 is restrained effectively, M135L-3 should be optimized further. However the J_b value of M135L-3 (2.512E-4 A/cm^2) is lower than that of M135L-5 (3.513E-4 A/cm^2) at whole perimeter-to-area range, indicating that the area-dependent leakage current of M135L-3 is reduced obviously maybe because the annealing treatment optimized the material. Especially, when the perimeter-to-area value is 200, the dark current density of M135L-3 is reduced about 45% from M135L-5. The curves about the dark current density and temperature of the photodiodes are shown in Fig.5. The dark current of M135L-3 photodiodes is obviously reduced, meanwhile the graph shows that the dark current of M135L-3 is lower than that of M135L-5 at whole temperature range. This may because the mesa is exposed to air for long time than M135L-5.

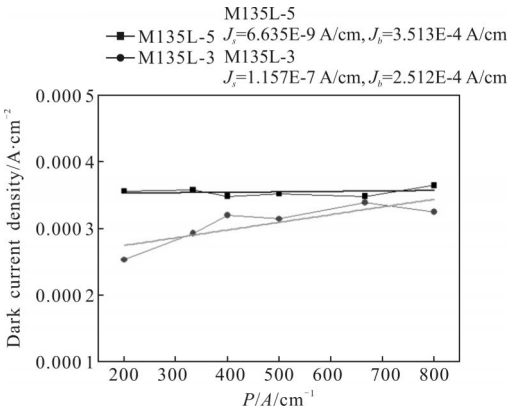

Fig.4 Dark current density vs P/A for M135L-5 and M135L-3 at room temperature (300 K)

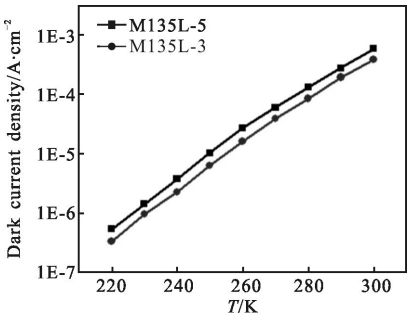

Fig.5 Dark current density and temperature

Thermal activation energy can be extracted by fitting the Eq. (7). The Arrhenius plots show the thermal activation energy (E_a) of M135L−3 in Tab.2. The dark current density versus the reciprocal of temperature of M135L−5 and M135L−3 measured at reverse 0.01−0.5 V bias are shown in Fig.6 and Fig.7, respectively. The results show that the dark current density is dominated by diffusion current for M135L−5 at 220−270 K at different bias voltages.

For the M135L−3, the dark current density is dominated by surface recombination current at 220−240 K at reverse bias 0.4−0.5 V, generation recombination current, ohmic leakage current and diffusion current at reverse bias 0.01−0.3 V at the same temperature, diffusion current at 250−280 K at different bias voltages.

Tab.2 Thermal activation energy E_a of M135L−3

	250−300 K	220−240 K
E_a(eV)@−0.5 V	0.347	0.162
E_a(eV)@−0.4 V	0.383	0.188
E_a(eV)@−0.3 V	0.4203	0.234
E_a(eV)@−0.2 V	0.455	0.313
E_a(eV)@−0.1 V	0.488	0.381
E_a(eV)@−0.01 V	0.500	0.343

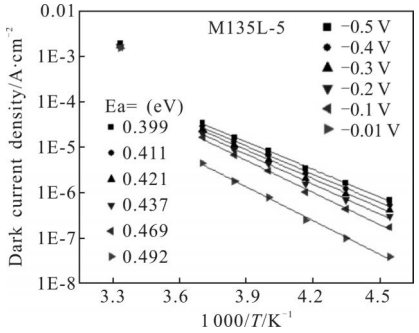

Fig.6 Dark current density of M135L−5 at different temperatures

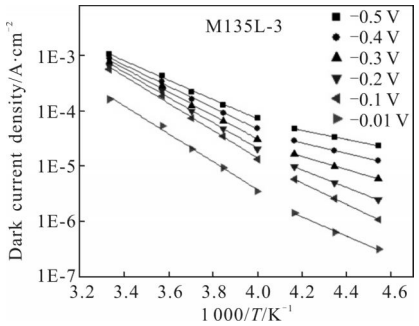

Fig.7 Dark current density of M135L−3 at different temperatures

However, the thermal activation energy is gradually decreased with increasing the reverse bias voltage for M135L−5, different form M135L−3. It concluded that the advantage for M135L−3 may result from its successful restraint of diffuse current at lower bias.

2.3 Fitting results of the dark current

The dark current measured and simulated for M135L−5 at 300 K and 220 K are shown in Fig.8. At 300 K, the results show that the dark current mechanisms are dominated by the diffuse current at relatively low reverse bias voltage, while the ohmic current (I_{ohm}) and the trap−assisted tunneling (TAT) current (I_{tat}) increase at relatively high reverse bias voltage. At 220 K, the dark current mechanisms are dominated by the GR (I_{g-r}) and ohmic (I_{ohm}) current at relatively low reverse bias voltage, while the TAT (I_{tat}) and ohmic current(I_{ohm}) increase at relatively high reverse bias voltage. The dark current measured and simulated for M135L−3 at 300 K and 220 K are shown in Fig.9. At 300 K, the results show that the dark current mechanisms are dominated by the diffuse and ohmic current at relatively low reverse bias voltage, while the ohmic current increases at relatively high reverse bias voltage. At 220 K, the dark current mechanisms are dominated by ohmic and GR current at relatively low reverse bias voltage, meanwhile dominated by TAT and ohmic current at relatively high reverse bias voltage. The results also show that the GR current and diffuse current of M135L−3 are lower compared with M135L−5 at 220 K.

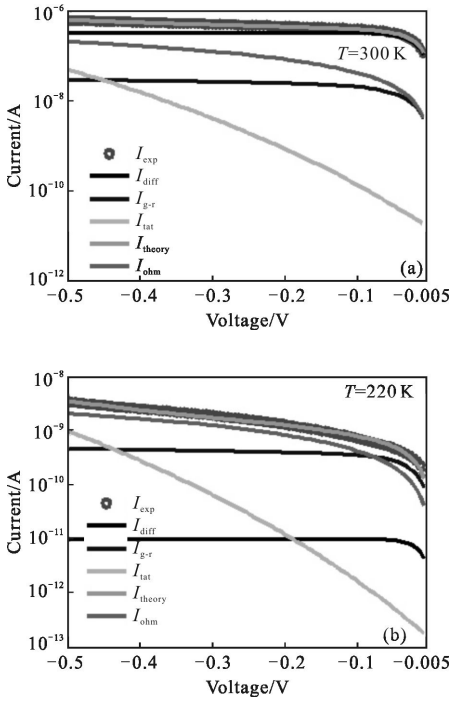

Fig.8 Dark current measured and simulated for M135L-5 at 300 K and 220 K

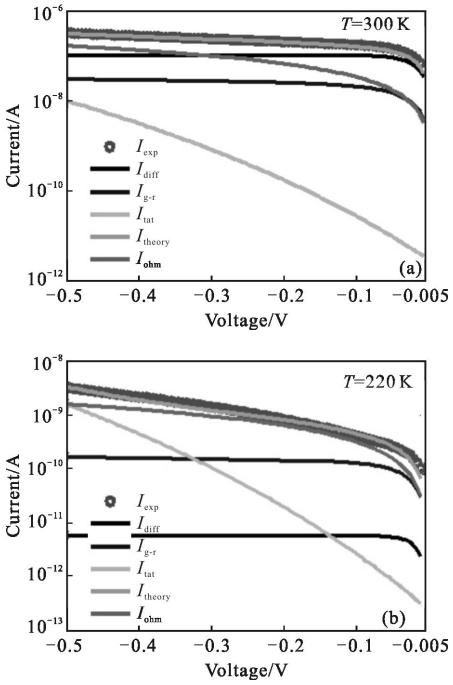

Fig.9 Dark current measured and simulated for M135L-3 at 300 K and 220 K

3 Conclusions

Two different annealing treatments for mesa type $In_{0.83}Ga_{0.17}As$ p-i-n photodiodes have been studied. The results show that the photodiodes with rapid thermal annealing before mesa etching has a lower dark current density at 220 K and 300 K, and the area-dependent leakage current has a lower level. The activation energy of both samples is extracted and the dark current is measured and simulated. The optimization of the photodiode performance is related to the decrease of sidewall recombination current. The annealing treatment mechanism for different anneal process need to be further researched.

References:

[1] Shi Yanli, Guo Qian, Li Long, et al. Visible-extended InP/InGaAs wide spectrum response infrared detectors [J]. ***Infrared and Laser Engineering***, 2015, 44(11): 3177-3180. (in Chinese)

[2] MacDougal M, Geske J, Wang C, et al. Low dark current InGaAs detector arrays for night vision and astronomy [C]// SPIE, 2009, 7298(3F): 1-10.

[3] Klem J F, Kim J K, Cich M J, et al. Mesa-isolated InGaAs photodetectors with low dark current [J]. ***Applied Physics Letters***, 2009, 95: 0311121-0311123.

[4] Jae-Hyung Jang, Student Member, Gabriel Cueva, et al. Metamorphic graded bandgap InGaAs -InGaAlAs -InAlAs double heterojunction P-i-I-N photodiodes [J]. ***Journal of Lightwave Technology***, 2002, 20(3): 507-514.

[5] Li Ping, Li Tao, Deng Shangyan, et al. Anneal treatment to improve the performance of extended wavelength $In_{0.83}Ga_{0.17}As$ photodetectors[J]. ***Infrared Phys Technol***, 2015, 71: 140-143.

[6] Cheng Jifeng, Zhu Yaoming, Tang Hengjing, et al. Microcosmic damage mechanism of inductively couple plasma etching for InGaAs [J]. ***Infrared and Laser Engineering***, 2013, 42(8): 2186-2189. (in Chinese)

[7] Anne Rouvie, Jean-Luc Reverchon, Odile Huet, et al. InGaAs focal plane arrays developments at III -V lab [C]//SPIE, 2012, 8353(8): 1-12.

[8] Li Y F, Tang H J, Li T, et al. Current-voltage characteristics of planar-type InGaAs infrared detectors [J]. ***Journal of Optoelectronics · Laser***, 2009, 20(12): 1580-1583.

[9] Zhou Yi, Chen Jianxin, Xu Qingqing, et al. Dark current analysis of long wavelength InAs/GaSb superlattice infrared detector[C]//SPIE, 2012, 8419(4): 1-7.